Simultaneous Kinetics and Ring-down: Rate Coefficients from Single Cavity Loss Temporal Profiles

Steven S. Brown,[†] A. R. Ravishankara,[‡,§,*] and Harald Stark[‡,||]

NOAA Aeronomy Laboratory, R/AL2, 325 Broadway, Boulder, Colorado 80303

Received: April 10, 2000; In Final Form: May 18, 2000

Cavity ring-down spectroscopy is a recently developed technique for highly sensitive detection of atomic and molecular absorptions. Here, we demonstrate the application of this technique to the measurement of kinetics that occur on the same time scale as the loss of light intensity from an optical cavity. We report rate constants for the reactions $NO + NO_3 \rightarrow 2NO_2$ and $OH + HNO_3 \rightarrow H_2O + NO_3$ at 296 K, measured as a test of this method. Observed ring-down profiles with a changing absorber concentration match calculated profiles, and fits to these profiles produce rate constants that agree with literature values to within the uncertainty of the measurements. The technique is general and should provide a simple means of measuring kinetic parameters for fast reactions. We also note the possible uses of this method for a variety of kinetics experiments and the outlook for future improvements.

I. Introduction

Flash-photolysis kinetic spectroscopy is a half-century-old tool for the measurement of reaction rate constants.[1] First invented by Porter and Norrish for studies of fast radical−molecule reactions, the technique originally used flash lamps to both photolytically produce and optically probe reactants and products, and a spectrograph with photographic plates as a detector. The idea was simply to measure a time-dependent absorbance by varying the delay between photolysis and probe flash lamps. Improvements in the methodology over the next decades included the use of monochromator-photomultiplier combinations, diode array spectrometers, CCD cameras, and, of course, laser light sources. These modifications improved the signal-to-noise and extended the technique to the study of a large number of systems, and further improvements continue to date. One of the key aspects of many such studies is the necessity to measure concentrations of a reactant or a product at discrete times following the initiation of a reaction, such that the duration for detection is negligible compared to the reaction time (i.e., the concentration of the probed species does not change during the detection period).

Cavity ring-down spectroscopy (CRDS)[2−5] is a recently developed technique for highly sensitive detection of gas-phase atomic and molecular absorptions. Since its invention twelve years ago,[2] it has seen increasingly widespread use. Injection of a laser light pulse into an optical cavity formed by two (or more) highly reflective mirrors leads to a single-exponential loss of light intensity via transmission through the end mirrors that can be monitored with a detector situated at the cavity output. The time constant for the empty cavity loss (τ_0) is variable, depending on the reflectivity of the mirrors but can range up to hundreds of microseconds.[6] The resulting effective path length traversed by the light is on the order of tens of kilometers, much longer than that achievable with a conventional absorption spectrometer even using a multipass cell. If an absorbing species of constant concentration is present in the ring-down cell, the intensity loss still follows a single-exponential decay but with a shorter time constant, τ. The difference between τ and τ_0 is directly related to the absorbance, α, the product of the absorber's number density and absorption cross section. The defining characteristic of CRDS is the transformation from the intensity domain, used for conventional absorption spectroscopy, to the time domain. Time domain measurement allows not only for the increased effective path length and consequent sensitivity but also for detection that is immune to noise fluctuations in the light source.

Cavity ring-down is an excellent detection method for measuring kinetics of radical species, particularly those that are not accessible via fluorescence excitation (i.e., molecules whose excited states predissociate or collisionally quench). The sensitivity of CRDS allows detection of radicals at concentrations low enough to suppress secondary chemistry such as self-reactions. Additionally, CRDS can easily be used as a detector in a pulsed-photolysis or discharge-flow configuration. Yu and Lin[7] pioneered the use of CRDS for kinetics measurements in 1993. Subsequently, Lin and co-workers used CRDS to measure kinetics of benzyl radical[8−16] and NH_2 radical[17] reactions. Atkinson and Hudgens used the same method to monitor reactions of ethyl radicals,[18] propargyl radicals,[19] and chloroallyl radicals,[20] and Atkinson *et al.*[21] studied IO kinetics. Zhu and co-workers have used CRDS detection to study HCO formation and loss after photolysis of several aldehydes,[22−25] and they have also investigated vinoxy radical reactions using CRDS.[26] Other recent applications have included vinyl radical absorption cross sections and kinetics,[27] HCO formation from reaction of $O(^3P)$ with alkenes,[28] and formation of BrO radicals.[29]

As noted above, any kinetic spectroscopy requires that the detection time be negligible compared to the reaction time. Because CRDS detection requires a finite time for photons to exit the cavity, the constraint for a kinetics experiment is that the absorber concentration not change significantly on the ring-

* To whom correspondence should be addressed.
† NOAA NRC Postdoctoral Fellow.
‡ Also affiliated with the Cooperative Institute for Research in Environmental Sciences, University of Colorado, Boulder, CO 80309.
§ Also affiliated with the Department of Chemistry and Biochemistry, University of Colorado, Boulder, CO 80309.
|| The listing of authors is alphabetical.

10.1021/jp0013715 CCC: $19.00
Published on Web 06/30/2000

down time scale. All of the aforementioned studies employed CRDS in this mode, using it as a sensitive detector to measure concentration at a series of discrete times after the photolytic initiation of a reaction. There is, however, another approach that to our knowledge has not been previously demonstrated: the case in which the concentration of the probed species changes on the ring-down time scale, i.e., the characteristic time for loss or formation is approximately equal to τ_0. In this configuration, the decay of light intensity out of the optical cavity is no longer a single exponential but rather a more complicated function of time that depends on the kinetics. There are several potential advantages to this approach. First, the entire measurement takes place in a single shot. Unlike a series of measurements taken at several discrete delay times after the generation of the absorbing species (for example by photolysis), a single ring-down temporal profile contains all of the relevant information; thus, it does not require, in many cases, that the initial concentration of the absorber be the same during the measurement of a temporal profile of the absorbing species. Second, the approach does not require that the absorber concentration be approximately constant on the ring-down time scale and, thus, does not limit the maximum measurable rate of the reaction. In contrast, it requires the concentration to change significantly during the ring-down process. As shown below, it is possible to extract kinetic parameters for an order-of-magnitude range of first-order (or pseudo first-order) rate constants near $1/\tau_0$. For the case of pseudo first-order kinetics, large first-order rate constants imply large concentrations of the excess reactant, ensuring that the pseudo first-order approximation is always valid. Third, the experiment is optimal under the condition of large τ_0 because there is no conflict between a large τ_0 value and the approximation that the absorber concentration remains constant on the time scale of τ_0. The highest sensitivity (and thus smallest absorber concentrations) occurs in the same regime as the most accurate kinetic measurements. Last, as discussed further below, this approach has potential applications to a variety of kinetic systems.

Because the kinetics and the ring-down occur simultaneously, we call the technique Simultaneous Kinetics and Ring-down, or SKaR. The next section develops expressions for light intensity time profiles for simultaneous reactive loss/formation and ring-down decay and shows the results for several different common rate expressions. All of the anticipated ring-down profiles are analytical functions. We then show how kinetic parameters can be extracted from the measured decays and present a general relationship between any observed ring-down decay and the time dependence of the absorber concentration. In the results section, we apply these models to measurement of the rate constants for two different reactions involving NO_3 radical.

$$NO_3 + NO \rightarrow 2NO_2 \qquad \text{(R1)}$$

$$OH + HNO_3 \rightarrow H_2O + NO_3 \qquad \text{(R2)}$$

Nitrate radical is a convenient target for SKaR measurements because of its strong absorption bands in the visible near 623 and 662 nm,[30] where high reflectivity (i.e., reflectivity, R, approaching 99.999%) mirrors are available. Reactions (R1) and (R2) have well-known rate constants and, thus, provide excellent model systems for kinetics experiments that measure the loss of reactant and the appearance of a product, respectively. Our SKaR measurements reproduce the literature values for the two rate constants, k_1 and k_2, to within the experimental uncertainty.

II. Model SKaR Profiles

The instantaneous loss rate of light intensity, I, propagating along the axis (defined below as the x-axis) of an optical cavity with a variable absorber concentration is given by the following expression.

$$\frac{dI}{dx} = -\alpha \cdot \frac{L_A}{L} \cdot I - \frac{T}{L} I \qquad (1)$$

Here, α is the absorbance, the product of the absorber number density and cross section (base e), T is the transmissivity ($1 - R$) of each mirror, assuming the cavity is composed of two identical mirrors, L is the cavity length, and L_A is the length over which the absorber is present. The first term in eq 1 is the Lambert−Beer Law. If L_A/L is less than unity, i.e., if the absorber is not present over the entire cavity length, the first term is an average of the loss due to absorption over the entire cavity length on each pass. The second term is an additional intensity loss that averages the discrete intensity loss that occurs at each encounter with the mirrors over the entire cavity length. Both terms in eq 1 are good approximations in the limit where the loss on a single pass can be represented differentially with respect to the overall loss process. For simplicity, we will assume L_A/L is unity in the following. Substitution into eq 1 of $dx = c\,dt$, where c is the speed of light, and $\tau_0 = L/cT$ gives

$$\frac{dI}{I} = -\left(c\alpha + \frac{1}{\tau_0}\right)dt \qquad (2)$$

If one assumes a constant absorber concentration, eq 2 yields the already well-known result for single-exponential intensity decay.[3,5]

$$I(t) = \exp\left(-c\alpha t - \frac{t}{\tau_0}\right) \qquad (3)$$

On the other hand, substitution into eq 2 of $\alpha = \alpha(t) = \sigma [A](t)$, where [A] is the absorber concentration, followed by integration gives

$$\ln\left(\frac{I(t)}{I_0}\right) = -c\sigma \int_0^t [A](t)dt - \frac{t}{\tau_0}, \text{ or} \qquad \text{(4a)}$$

$$I(t) = I_0 \exp\left[-c\sigma \int_0^t [A](t)dt - \frac{t}{\tau_0}\right] \qquad \text{(4b)}$$

Here, I_0 is the intensity at time zero, which may be any arbitrary time during the course of the decay. Equation 4 is a general expression for $I(t)$ because we have not yet specified the form of $[A](t)$. We now derive expressions for $I(t)$ in some frequently encountered kinetics cases.

Case A: First-Order Loss. Perhaps the most common kinetics experiment is the measurement of a first-order (or pseudo first-order in the case of a bimolecular reaction) disappearance of a reactant. In this case, the absorbing species has a single-exponential loss, $[A](t) = [A]_0 \exp(-k' t)$, where $[A]_0$ is the initial reactant (absorber) concentration and k' is the first-order rate constant. Substitution of this equation into (4) and integration gives the following expression for $I(t)$.

$$I(t) = I_0 \exp\left[-\frac{c\alpha_0}{k'}(1 - e^{-k't}) - \frac{t}{\tau_0}\right] \qquad (5)$$

Here, $\alpha_0 = \sigma [A]_0$ is the absorbance at $t = 0$. In this case, the

decay at short times (where $1 - e^{-k't} \approx k't$) matches that of a cavity with a time-independent absorbance α_0, and at long times (where $1 - e^{-k't} \approx 1$) goes to the empty cavity decay (i.e., $I_0 \exp(-t/\tau_0)$ with the intensity reduced by a constant factor of $\exp(-c\alpha_0/k')$. Thus, in principle, if one knew α_0 independently, one could roughly estimate the rate constant k' simply from the long-time ratios of the signals.

Case B: First-Order Production. If the absorber is not a reactant but rather a product of a first-order reaction, one may also measure the first-order rate constant from the product appearance. In this case, the time dependence of the absorber concentration is $[A](t) = [A]_\infty(1 - e^{-k't})$, where $[A]_\infty$ is the product concentration after the reaction has gone to completion. Substituted into eq 4, this form of [A](t) gives

$$I(t) = I_0 \exp\left[-\left(c\sigma_\infty + \frac{1}{\tau_0}\right)t + \frac{c\alpha_\infty}{k'}(1 - e^{-k't})\right] \quad (6)$$

As above, $\alpha_\infty = \sigma [A]_\infty$. In this case, as expected, the decay behaves like that from an empty cavity at short times and goes to the single-exponential decay of the empty cavity plus the absorber at long times.

Case C: Consecutive First-Order Production and First-Order Loss. In the case where the monitored species arises from first-order production (with a first-order rate constant, k_P'), there is typically a first-order loss (with a first-order rate constant, k_L') that one must also account for in order to determine k_P'. The following two equations give the absorber concentration, [A](t), for the case of such consecutive reactions and the resulting $I(t)$ from eq 4, respectively.

$$[A](t) = [X]_0 \left(\frac{k_P'}{k_P' - k_L'}\right)[\exp(k_L't) - \exp(k_P't)] \quad (7)$$

$$I(t) = I_0 \exp\left\{-c\sigma_0\left(\frac{1}{k_L'(k_P' - k_L')}\right)[k_P'(1 - e^{-k_L't}) - k_L'(1 - e^{-k_P't})] - \frac{t}{\tau_0}\right\} \quad (8)$$

In eq 7, $[X]_0$ is the initial concentration of the limiting reactant. In eq 8, α_0 is the product of σ (the absorption cross section of the reaction product, A) and $[X]_0$, which is nearly the same as the parameter α_∞ for case B above if k_L' is much less than k_P' (i.e., the loss is small compared to production). If k_L' is comparable to k_P', then the α_0 parameter in eq 8 will be significantly smaller than the α_∞ parameter in eq 6.

Analytical expressions for other rate laws can be derived. For example, the expression for a second-order loss of a reactant/absorber following the rate expression $[A](t) = [A]_0/(1 + kt[A]_0)$ is

$$I(t) = I_0 \exp\left[-\frac{c\sigma}{k}\ln(1 + kt[A]_0) - \frac{t}{\tau_0}\right] = I_0 (1 + kt[A]_0)^{-c\sigma/k} e^{-t/\tau_0} \quad (9)$$

However, this kinetics case has not been demonstrated here.[31]

The expressions in eqs 4−9 are analytical, and one could, in principle, fit observed ring-down temporal profiles directly to them. However, definition of a function Ratio(t) that is the ratio of the intensity profile with kinetics to that measured for the empty cavity (i.e., no absorber) simplifies the data analysis and makes the fit more robust.

$$Ratio(t) = \frac{I(t)}{I_0 e^{-t/\tau_0}} = \exp[-c\sigma \int [A](t)dt] \quad (10)$$

Because the denominator in eq 10 is just the empty cavity profile, it is easily measured experimentally, and one need only take the ratio of two measured ring-down profiles to generate this function. For each of the cases described above, the ratio is given by the following expressions.

First-order loss:

$$Ratio(t) = \exp\left[-\frac{c\alpha_\infty}{k'}(1 - e^{-k't})\right] \quad (10a)$$

First-order production:

$$Ratio(t) = \exp\left\{-\frac{c\alpha_\infty}{k'}[k't - (1 - e^{-k't})]\right\} \quad (10b)$$

Consecutive first-order production and first-order loss:

$$Ratio(t) = \exp\left\{-c\alpha_0\left(\frac{1}{k_2'(k_1' - k_2')}\right)[k_1'(1 - e^{-k_2't}) - k_2'(1 - e^{-k_1't})]\right\} \quad (10c)$$

Fits to eq 10a − c remove the dependence of the observed ring-down on the empty cavity decay time and the initial intensity present in eq 5−9. Examples of experimental observation and fits to Eq 10 a−c appear in the Results section.

Finally, it is worth noting that the method outlined above is general and, in principle, does not require an analytical function for the time dependence of the absorber concentration, [A](t). The measured ring-down profiles yield the temporal profile of the absorber directly since the time derivative of the logarithm of eq 10 recovers [A](t).

$$\ln[Ratio(t)] = -c\sigma \frac{L_A}{L} \int [A](t)dt \quad (11)$$

$$\frac{d\ln[Ratio(t)]}{dt} = -c\sigma \frac{L_A}{L}[A](t) \quad (12)$$

$$[A](t) = \frac{1}{c\sigma}\frac{L}{L_A}\frac{d\ln[Ratio(t)]}{dt} \quad (13)$$

Here, we have explicitly included the factor L_A/L from eq 1. Clearly, if desired, one could extract an arbitrary time profile of absorber concentration in absolute units from observed ring-down intensity profiles in the presence and absence of the absorber. We demonstrate the calculation of the absolute concentration temporal profiles from eq 13 at the end of the next section. In practice, the [A](t) profiles from eq 13 depend on the accuracy of the numerical differentiation step. Thus, a fit to eq 10 is likely to be a more accurate method to determine rate constants where analytical integration of [A](t) is possible.

III. Demonstration of Rate Constant Measurement

Experiments. The CRDS apparatus has been described previously.[32] Here, we detail only the changes necessary to obtain kinetic data on NO_3 radicals produced upon photolysis and undergoing reactions on the time scale of the CRDS experiment. A Nd:YAG laser pumped dye laser tuned to either 623 or 662 nm with a pulse duration of 6−8 ns was used for measuring ring-down signals. The intensity of light escaping from the rear mirror was collected by a PMT, digitized in an

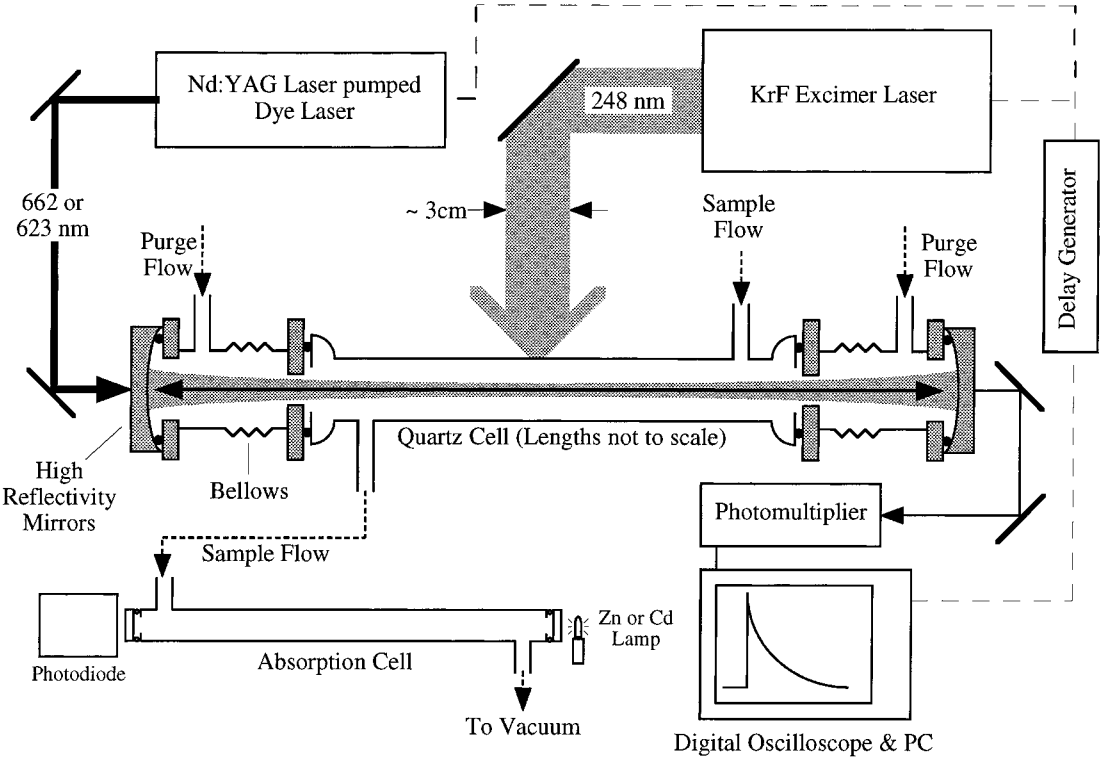

Figure 1. Schematic of the experimental apparatus used to measure the temporal profile of a reactant or a product on the time scale of the ring-down signal.

oscilloscope, and processed in a computer. The high reflectivity mirrors used in this work resulted in empty cavity ring-down time constants (τ_0) between 100 and 160 μs, depending on the wavelength of the light. These τ_0 correspond to mirror reflectivities of 99.997% and 99.998%.

Figure 1 shows a schematic of the experiment modified for the photolysis experiments. This apparatus is nearly identical to the one described in our previous paper,[32] with the exception of the inclusion of a photolysis pulse orthogonal to the ring-down beam. This arrangement is similar to the apparatus of Atkinson et al.[18,19,21] A KrF excimer laser produced UV light pulses with duration of 10−20 ns at 248 nm. The output energy of the laser was ~100 mJ per pulse. The beam was attenuated by quartz filters to the desired pulse energies. A cylindrical lens ($f = 1$ m) shaped the photolysis beam into a 0.5 × 3 cm ribbon of light aligned to the axis of the reactor. The ring-down beam passed through the middle of this photolysis volume. As shown in the figure, the cell consisted of a purge volume at each end and a quartz tube in the center. The purge volumes efficiently suppressed contamination of the mirrors from exposure to corrosive gases such as nitric acid. This was demonstrated by the value of τ_0 measured before being the same as that obtained after the introduction of gases such as HNO_3 and N_2O_5.

The overall path length of the cell was 95 cm. The total pressures in all experiments varied between 12 and 200 Torr. Calibrated mass flow meters measured the gas flows, which determined the concentrations of the radical precursor and the linear flow velocities of the gases through the reactor. An absorption cell located downstream from the ring-down cell was used to measure the concentration of N_2O_5 or HNO_3 radical precursors. During all the measurements reported here, we monitored the NO_3 radical at either 623 or 663 nm, where its absorption cross sections are 1.5 and 2.2 × 10^{-17} cm^2 molecule^{-1},[30] respectively. All experiments were carried out at room temperature, 296 ± 2 K.

To measure k_1, the rate constant for (R1), NO_3 was generated by 248 nm photolysis of N_2O_5. The absorption cross section of N_2O_5 at 248 nm is 4.5 × 10^{-19} cm^2 molecule^{-1},[33] with a quantum yield near unity.[34,35] The initial concentrations of NO_3 produced from photolysis were in the range of 0.4 to 4 × 10^{12} cm^{-3}. It was necessary to minimize the NO_2 concentration, which was present as an impurity in NO or was produced due to the thermal decomposition of N_2O_5. The NO_2 in NO was removed by using a trap maintained at 195 K and located between the bulb containing NO and the reaction cell. The resulting NO_2 concentration was $<10^{11}$ molecules cm^{-3} in the reactor as measured by the maximum change in τ_0 upon addition of NO to the ring-down cell. Thermal decomposition of N_2O_5 produced both NO_2 and NO_3. The NO_3 reacted with NO to produce two additional NO_2 molecules. The resulting concentration of NO_2 did not significantly reduce the empty cavity ring-down time constant. The reaction sequence consumed less than 3% of the NO even at the lowest [NO] and the highest [N_2O_5]. Thus, the flow measurement was an accurate determination of the NO concentration despite the presence of this reaction sequence.

To measure k_2, the rate constant for reaction (R2), nitric acid served as both the excess reactant and the photolytic precursor for OH radicals. A bubbler containing liquid nitric acid was maintained between 278 and 298 K, and a variable carrier gas flow passed through it to obtain gas-phase concentrations of HNO_3 between 1 and 7 × 10^{16} molecules cm^{-3} in the reactor. Alternatively, we used a temperature-controlled trap with a flow of carrier gas passing over the liquid surface to draw away HNO_3 vapor. The latter source produced smaller gas-phase NO_2 contamination, but controlling the HNO_3 concentration was more difficult. Both sources gave total NO_2 concentrations (measured as above by observation of the change in the ring-down time constant upon addition of HNO_3 to the empty cavity) of less than 4 × 10^{-5} times that of the gas-phase nitric acid concentra-

tion, similar to our previous observations.[36] The low NO_2 contamination level was not sufficient to affect the measurement of k_2.

The delay between photolysis and ring-down laser was controlled by a home-built, computer-controlled device. The repetition rate of the lasers was 10 Hz while measuring k_1. To record the empty cavity ring-down signals, the excimer laser was fired 1.5 ms after the ring-down laser. To obtain kinetic information, the excimer laser fired about 10 μs after the ring-down laser. The repetition rate for measuring k_2 had to be smaller (1−2 Hz) in order to allow the gas flow to completely remove the reaction products in the time between successive laser shots. In both experiments, we averaged 128 to 256 individual temporal profiles.

N_2O_5 and anhydrous HNO_3 were synthesized, stored, and handled by methods described previously,[37,36] with the exception that we added a small amount of water to the anhydrous liquid HNO_3 to suppress N_2O_5 formation. The N_2O_5 concentrations in the reactor for studies of reaction (R1) were measured by absorption in a 100 cm long cell at 228 nm (Cd lamp), in which the cross section was 1.2×10^{-18} cm^2 molecule^{-1}.[33] The HNO_3 concentrations were similarly measured in a 50-cm cell using a zinc lamp at 213.9 nm ($\sigma(HNO_3) = 1.54 \times 10^{-19}$ cm^2 molecule^{-1}).[38] NO was purified by passing it through a silica gel filled glass trap maintained at 155 K before filling a 12 L glass bulb and diluting it (to 5%) with nitrogen.

Results

Reaction (R1), $NO + NO_3 \rightarrow 2\ NO_2$. The rate coefficient, k_1, was determined by observing the temporal behavior of NO_3 reactant during the ring-down time in the presence of various concentrations of NO. The concentration of NO was always much larger than that of NO_3; thus, the rate of NO_3 loss was first-order in $[NO_3]$. The first-order rate coefficient for the decay of NO_3 was

$$k_1' = k_1\,[NO] + k_d \qquad (14)$$

where k_d is the first-order rate coefficient for the loss of NO_3 due to the removal from the observation zone and due to reactions other than reaction (R1).

As explained earlier, acquisition of two ring-down signals, one with and one without the absorber, simplified the determination of rate constants, as shown in Figure 2. The upper signal in Figure 2a shows the ring-down intensity profile in the absence of NO_3 but with N_2O_5 and NO flowing through the cell. As seen in the figure, the empty cavity ring-down was strictly exponential over 3 orders of magnitude in intensity. Therefore, the ring-down time constant in the absence of NO_3 production was well defined and provided the value of τ_0. The lower signal shows a ring-down profile in which the NO_3 concentration was changing due to its reaction with NO after its production via N_2O_5 photolysis. The nonexponential behavior of the ring-down signal is readily apparent on the logarithmic scale of the figure. The slope at long times is the same as τ_0 because NO_3 had been removed due to reaction (R1).

Figure 2b shows the ratio of the two ring-down signals shown in Figure 2a. The ratio is described by eq 10. The start of the reaction, i.e., the photolytic production of NO_3, is clear from the discontinuity in Figure 2b. The ratio remains at unity until the photolysis pulse; it changes instantaneously due to photolytic production and then more slowly because of loss of NO_3 via reaction (R1). The scatter in the ratio at longer times limits the observation time to approximately 300 μs in this case. This time

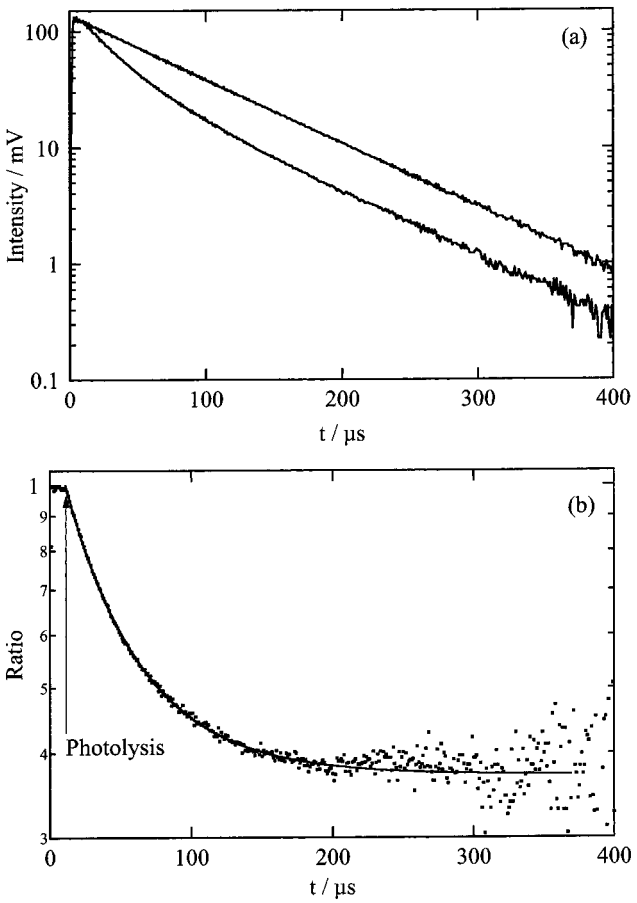

Figure 2. (a) Ring-down temporal profiles in the absence (upper trace) and presence (lower trace) of NO_3 radicals whose concentration is changing due to reaction (R1). (b) Ratio of the lower to the upper trace from plot (a) (points) along with a fit to eq 10a (solid line). The discontinuity that occurs at 12 μs (arrow) results from photolytic production of NO_3 from N_2O_5, and the somewhat slower return to a horizontal line is due to reactive NO_3 loss.

scale depends on the initial NO_3 concentration and the loss rate constant for NO_3, k_1'. Longer times were achieved at smaller initial NO_3 concentrations and larger k_1' (high NO concentration). It should be noted that with a better transient digitizer and more signal averaging, the usable time scale could be extended. (We used an 8-bit digitizer.)

The measured ratio was fit to eq 10a using the Levenberg−Marquardt algorithm and is shown as the solid line in Figure 2b. Varying the k_1' value by more than ±5% gave a clearly poorer fit, and thus demonstrated the sensitivity of this ratio to the determined pseudo first-order rate constant. We fixed the zero time at the measured value in these fits and allowed the two fit parameters, k' and α_0, to vary.[39] A variation in the time limits over which the fit was carried out gave an estimate of the uncertainty associated with k'. For example, a series of fits to the data in Figure 2b beginning at the photolysis pulse and ending at different times between 200 and 350 μs produced slightly different k' values, although the dependence of the end limit on the fit was not systematic. For each ratio, we carried out a series of fits over the appropriate time limits and took the resulting average and standard deviation as $k' \pm \sigma$. The standard deviations generally fell in the range of ±5% of the k' values (see Table 1).

Figure 3a shows plots of the temporal profile of the ratio for a few concentrations of NO. Here, k_1' values varied between 5000 s^{-1} to 55 000 s^{-1}. The results of all of the measurements

TABLE 1: Pseudo First-order Rate Constants for Reaction (R1)[a]

No.	[NO]/10^{14} molecules cm^{-3}	$k_1'/10^3$ s^{-1}	$\alpha_0/10^{-7}$ cm^{-1}
1	8.20	24.0 ± 1.2	8.00 ± 0.16
2	13.5	36.5 ± 0.6	11.8 ± 0.1
3	3.30	9.9 ± 0.9	3.56 ± 0.09
4	16.8	44.4 ± 1.9	14.3 ± 0.3
5	10.2	28.1 ± 0.2	9.53 ± 0.03
6	4.89	14.8 ± 1.1	5.22 ± 0.12
7	1.60	5.0 ± 0.7	1.88 ± 0.05
8	11.9	32.8 ± 0.4	11.0 ± 0.1
9	15.0	40.9 ± 1.0	13.3 ± 0.1
10	20.0	53.5 ± 1.9	17.1 ± 0.3
11	6.55	19.1 ± 0.6	6.70 ± 0.07
12	6.63	18.8 ± 0.1	7.17 ± 0.05
13	6.70	19.2 ± 0.1	8.64 ± 0.05
14	6.68	18.4 ± 0.2	5.57 ± 0.05
15	6.66	18.7 ± 0.2	3.87 ± 0.05
16	6.63	18.5 ± 0.3	2.06 ± 0.04
17	6.56	18.3 ± 0.1	6.26 ± 0.05

[a] $T = 296 \pm 1$ K, $P = 50 \pm 2$ Torr, Bath gas = N_2.

are summarized in Table 1, along with the pertinent experimental conditions. Figure 3b shows a plot of the measured pseudo first-order rate constants, k_1', as a function of NO concentration. Clearly, k_1' varies linearly with [NO], and the slope of the line is the second-order rate constant k_1. The slope was derived from a linear least-squares fit of the k_1' vs [NO] data to eq 14 to obtain k_1:

$k_1 = (2.6 \pm 0.2) \times 10^{-11}$ cm^{3}molecule^{-1}s^{-1}

The evaluated value for reaction (R1) is 2.6×10^{-11} cm^{3}molecule^{-1}s^{-1} at 298 K.[40] The quoted error limits in our measurement are at the 95% confidence level and include the precision of the slope from the fit plus additional estimated systematic errors. The intercept, k_d, in the above analysis was (1800 ± 600) s^{-1}. Although this intercept appears to be large, it is quite small compared to the range of k_1' values measured (see Figure 3b). Any small changes in k_d did not significantly affect the derived value of k_1. We attach no significance to its value being nonzero. Possible systematic errors in the NO concentration measurements include calibration errors from mass flow meters and pressure gauges (±6%) plus reactive loss of NO with the NO_3 from thermal decomposition of N_2O_5 (±3%), described above.

During most of the measurements (e.g., all of the points in Figure 3b), the ratio $[NO_3]_0/k_1'$was held roughly constant by maintaining a constant ratio between the NO flow and the flow through the N_2O_5 reservoir. This procedure resulted in values of 0.95 to 1.05 for $c\alpha_0/k_1'$ in eq 10a. Because the ratio of the signal to the background trace is $\exp(-c\alpha_0/k_1')$ at long times, holding this ratio approximately constant ensures that all ratio signals approach the same value (see Figure 3b). Thus, the observation time is roughly constant at all $[NO_3]$ values, and the fits to the data are more robust because we fix $\exp(-c\alpha_0/k_1')$ to lie at reasonable values, i.e., in the range 0.32−0.38. In a related set of experiments, we varied $[NO_3]_0$ over a factor of 4 at fixed [NO] (or k_1') to check for influence of this variation on the measured rate constant; there was no systematic variation of k_1' with α_0 (see measurement nos. 11−17 in Table 1).

Reaction (R2), OH + HNO_3 → H_2O + NO_3. The temporal profile of NO_3, the product of reaction (R2), was monitored to measure k_2. Because $[OH]_0$ was much less than $[HNO_3]$, the reaction was first-order in [OH]. The temporal profile of NO_3 product, therefore, was given by the first-order rate constant for the loss of OH. If NO_3 was not lost by any process after its production, we should have observed a ratio given by eq 10b. However, if there was a removal process for NO_3, the temporal profile of NO_3 would have been an example of consecutive reactions and would have been represented by eq 10c.

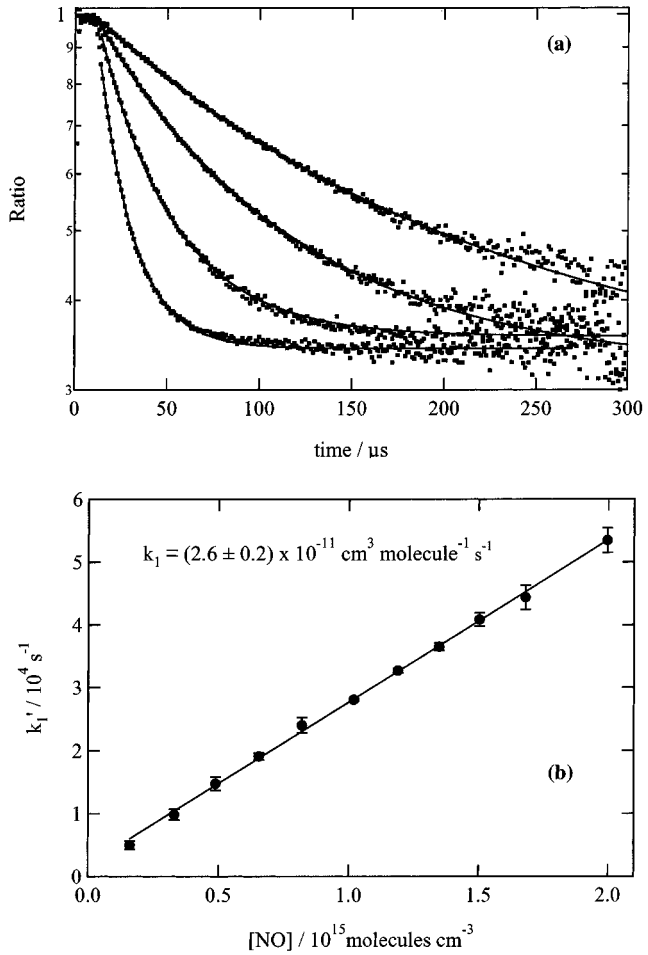

Figure 3. (a) Series of experimentally determined ratios (points) as described by eq 10a for the loss of NO_3 radicals via reaction (R1). Each trace occurs at a different NO concentration and therefore a different pseudo first-order rate constant, k_1'. The solid lines are fits of each trace to eq 10a. (b) Plot of best fit value for the pseudo first-order rate constant, k_1', vs measured NO concentration. The slope of this plot is the bimolecular rate constant, k_1, for the reaction $NO_3 + NO \rightarrow 2NO_2$.

Figure 4a shows a typical ring-down signal. As the reaction proceeds, the buildup of NO_3 is evident by the monotonically increasing slope of the ring-down signal. At longer reaction times, the NO_3 concentration reaches its maximum value and the slope becomes nearly constant. If NO_3 is not lost via a reaction on the time scale of the experiments, this value would be constant and only the physical removal from the cell would constitute a loss. For comparison, the empty cavity ring-down profile is also shown. This profile was obtained by firing the photolysis laser 2−3 ms after the ring-down laser with HNO_3 present in the cell. Clearly, the initial ring-down time constants are the same in both the profiles. When NO_3 generation begins, the second profile shows the continuously decreasing ring-down time constants as the concentration of NO_3 increases in the reactor.

Figure 4b shows the ratio of the ring-down profiles with and without NO_3 generation. Even at the low repetition rates used in this experiment, the NO_3 from the previous pulse was not completely removed from the cell, as evidenced by a slight reduction in the ring-down time constant relative to the one obtained in an empty cavity. The observed removal rate of NO_3

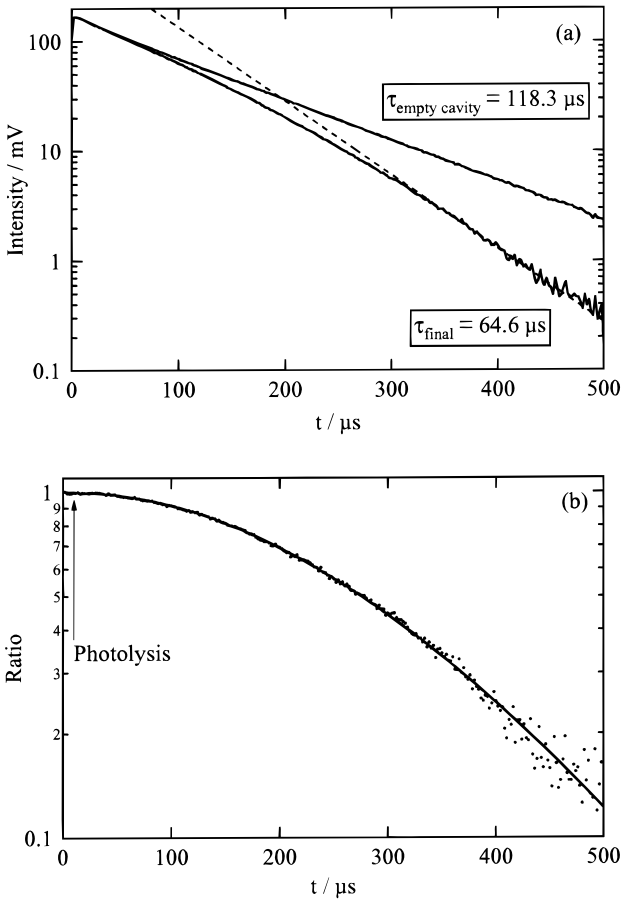

Figure 4. (a) Ring-down temporal profiles in the absence (upper trace) and presence (lower trace) of NO_3 radicals whose concentration is changing due to production via reaction (R2). The initial slope in the lower trace is the same as that for the empty cavity, and the slope at long time is due to the empty cavity loss plus the final, approximately constant, NO_3 absorption, as the dashed line shows. (b) Ratio of the lower to the upper trace from plot (a) (points) along with a fit to eq 10b (solid line). The arrow marks the time at which the photolysis laser produced OH radicals.

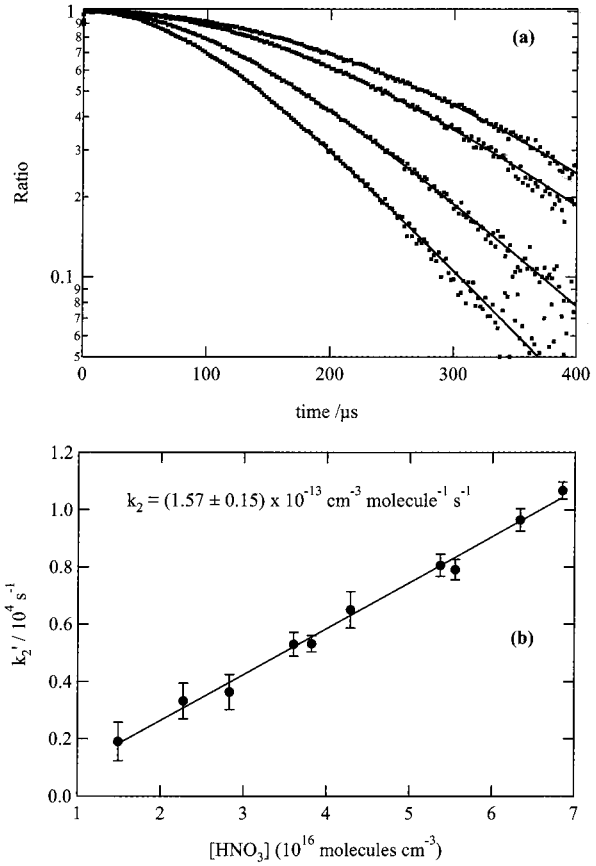

Figure 5. (a) Series of experimentally determined ratios (points) as described by eq 10 for the production of NO_3 radicals via reaction (R2). Each trace occurs at a different HNO_3 concentration and, therefore, a different pseudo first-order rate constant, k_2'. The solid lines are fits of each trace to eq 10b. (b) Plot of best fit value for the pseudo first-order rate constant, k_2', vs measured HNO_3 concentration. The slope of this plot is the bimolecular rate constant, k_2, for the reaction OH + HNO_3 → H_2O + NO_3.

was sufficiently slow under constant flow conditions to justify the assumption of a small steady background NO_3 concentration.

In a separate set of experiments, the slow loss of NO_3 after its production was measured by recording the ring-down time constants at a series of discrete delays between the photolysis and the ring-down laser pulses after the completion of reaction (R2). This experiment, carried out with delays of milliseconds, was much the same as "conventional" photolysis-CRDS experiments.[7,18,26] The time constant for the slow NO_3 removal determined by this method was ≈20 s^{-1}, much smaller than the rise times measured for reaction 2.

The data, such as those shown in Figure 4b, were fit to both eq 10b and 10c using the nonlinear least squares procedure described earlier. For fits to eq 10c, the temporal profile of NO_3 is given by eq 7 with k_2' replacing k_P'. The rough estimates of the errors in obtained values of k_2' were obtained in the same way as in the determination of k_1' (above). The value for k_L' was kept constant for all fits, whereas the two other fitting parameters k_2' and α_0 were varied. The result of using eq 10c was to yield slightly larger values of k_2' than those obtained by fitting to eq 10b, although the difference is well within the uncertainty of the fits.

Figure 5a shows four ring-down profiles in which [NO_3] varied due to its production via reaction (R2). The solid lines are fits to eq 10b. Table 2 lists the values of k_2' determined in this study, along with other pertinent experimental conditions. The range of the first-order rate constants measured here were 2000−11 000 s^{-1}. We could not measure larger values because the maximum [HNO_3] was limited by its vapor pressure.

TABLE 2: Pseudo First-order Rate Constants for Reaction (R2)[a]

No.	[HNO_3]/10^{16} molecules cm^{-3}	$k_1'/10^3$ s^{-1}	$\alpha_\infty/10^{-7}$ cm^{-1}
1	2.33	3.53 ± 0.29	3.30 ± 0.24
2	4.39	6.61 ± 0.27	2.45 ± 0.06
3	6.49	9.83 ± 0.18	2.8 ± 0.03
4	5.70	8.23 ± 0.16	4.68 ± 0.06
5	2.90	3.78 ± 0.30	5.07 ± 0.34
6	1.53	2.04 ± 0.33	4.14 ± 0.64
7	3.69	5.47 ± 0.18	3.41 ± 0.08
8	5.50	8.20 ± 0.12	3.16 ± 0.02
9	7.02	10.82 ± 0.29	3.79 ± 0.02
10	3.85	5.60 ± 0.24	3.48 ± 0.11

T = 296 ± 1 K, P = 68−75 Torr, Bath gas = N_2.

Figure 5b shows a plot of the measured first-order rate constant as a function of [HNO_3]. The slope of this plot gives a bimolecular rate constant

$k_2 = (1.57 \pm 0.15) \times 10^{-13}$ cm^3 $molecule^{-1}$ s^{-1}.

Our previous result for reaction R2 gave 1.44×10^{-13} cm^3 $molecule^{-1}$ s^{-1} at the same temperature and pressure.[36] The value of k_d was essentially zero (−399 ± 377 s^{-1}). The quoted error limits are at 95% confidence limit of the slope of the linear least-squares fit and the estimated systematic errors in the

$[HNO_3]$ measurements including flow meter calibrations (±6%) and uncertainties in the HNO_3 cross section at 214 nm (±4%).[35]

It is known that NO_3 is produced vibrationally hot in the photolysis of N_2O_5 and may also be excited in reaction 2. If vibrationally excited NO_3 relaxes to the ground state during the measurements of k_1 and k_2, the obtained values of the rate coefficients will be in error. However, Torabi[41] has shown that the relaxation of NO_3 (produced by N_2O_5 photolysis) is essentially complete in 7 μs in the presence of about 50 Torr of He. Thus, only the first 3 or 4 points in an experimental signal can be influenced by vibrational relaxation, and these points were excluded from the fit.

IV. Discussion and outlook

The comparison between our measured values and previous studies show the validity of the SKaR method for measuring rate coefficients using cavity ring-down when the concentration of the absorber is changing on the ring-down time scale. Our measured value of k_1 is in excellent agreement with the evaluated value.[40] The rate coefficient for reaction (R1) is large, independent of pressure and essentially independent of temperature. Therefore, our measurements near room temperature in approximately 50 Torr of N_2 can be compared with the literature values. Our measured value of k_2, which varies with pressure and temperature, can be compared with the recent measurement from our laboratory.[36] Under comparable pressure and temperature conditions, our value is essentially the same as our previous result.

As mentioned above, a measured ring-down profile can be converted to a temporal profile of the absorber using Eq 13. To demonstrate this principle, Figure 6 shows two such plots of the derived NO_3 concentration profiles, one for reaction (R1) and another for reaction (R2). The solid lines in Figure 6, parts a and b, are calculated NO_3 profiles from the fitted values for α_0 and k′ obtained from the analysis of eq 10 described in the preceding section. The agreement between the lines and the data is good despite the large scatter. The main reason for this scatter is the differentiation of the data with rather coarse time steps of 1 μs. However, it is clear that the temporal profile of the absorber can be obtained. The quality of the derived concentration profiles can be improved using finer time resolution, higher digitization resolution, larger laser intensity, and higher signal averaging.

The empty cavity ring-down time constant, τ_0, determines the range of pseudo first-order rate constants measurable with the SKaR method. In our system, with a mirror reflectivity of about 99.998% ($\tau_0 \approx 150$ μs) and a base path length of ≈100 cm, the maximum overall detection time was ≈500 μs. We have showed here that pseudo first-order rate constants between 1000 and 60 000 s^{-1} can be measured with the SKaR method. Future improvements in mirror technology will improve the versatility of the technique. Elongating the cavity and using only a small part of the cavity for chemical reactions will extend this duration significantly. Therefore, we anticipate obtaining observation times of a few milliseconds and thus reducing the smallest measurable first-order rate constants to a few hundred per second. The largest first-order rate constants that can be measured will be controlled by the limitations inherent in many kinetics systems such as thermalization of the reactants and concentrations of reagents that can be used. Studies of second order reactions are likely to be more limited as discussed in section II. In the present study, in which the photolysis and ring-down laser beams were orthogonal, radicals were present only over a small length of the cavity (small value for L_A/L).

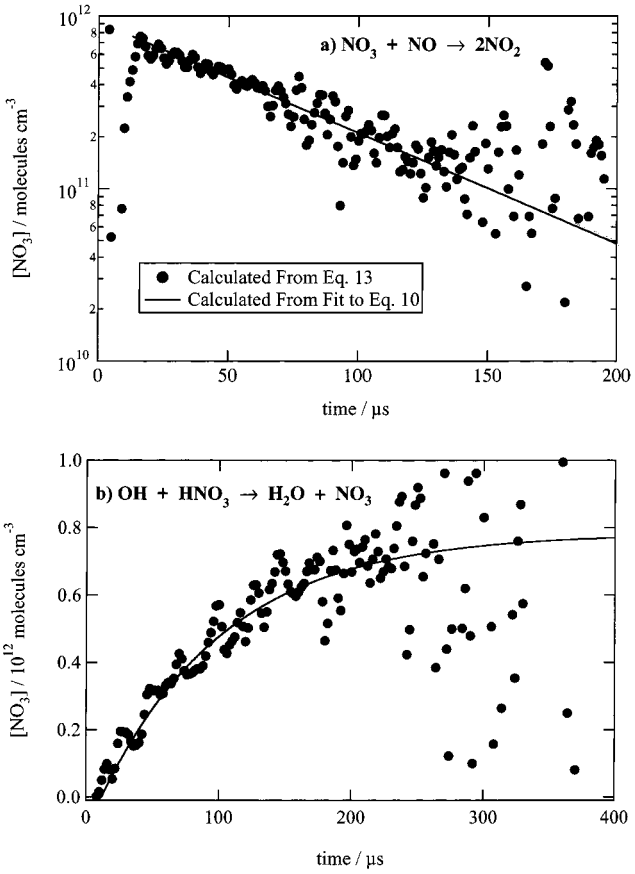

Figure 6. (a) Direct inversion of an observed ring-down profile (points) to yield absolute $[NO_3](t)$ according to eq 13 for NO_3 loss due to reaction (R1). We smoothed the data by a factor of 3 prior to differentiation to reduce scatter. This smoothing introduced the unrealistic rise that is not seen in the observed profile (Figure 2b). The rise also has a small contribution from the relaxation of vibrationally excited NO_3 produced by N_2O_5 photolysis (see text). The line is a calculated NO_3 profile based on best fit values for k_1' and $[NO_3]_0$ from eq 10. (b) Same plot as in (a) except for NO_3 production via reaction (R2).

Future improvements to our apparatus will include crossing the laser beams at a small angle to improve the overlap and thus the detection sensitivity.

It is also worth noting that fitting the ring-down profiles to a simple kinetics scheme leads to high quality data because the whole profile is utilized. Therefore, the method used here may be a better way to extract rate data when the rate expression for the reaction can be analytically solved. However, it should also be possible to numerically integrate a set of reactions and obtain a temporal profile that can be converted to a ring-down signal. Then, one could carry out a fit of a ring-down profile to any arbitrary sequence of reactions that make up a specific mechanism.

The SKaR method should find applications in situations where the generation of the experimental conditions such as temperature, pressure, and composition cannot be maintained for long periods of time. Examples include shock tubes for high temperature studies, a Laval nozzle or pulsed beam for very low temperature measurements, and IR laser heating for high temperature studies. Also, it may be possible to follow the evolution of transient species, such as vibrationally excited molecules using the SKaR technique.

Acknowledgment. H.S. thanks the Deutsche Forschungsgemeinschaft for a research fellowship, and S.S.B. thanks the

National Research Council for a postdoctoral fellowship. This work was funded in part by NOAA's climate and global change program and in part by NOAA's health of the atmosphere program.

References and Notes

(1) Porter, G. *Proc. R. Soc. London Ser. A.* **1950**, *200*, 284.
(2) O'Keefe, A.; Deacon, D. A. G. *Rev. Sci. Instrum.* **1988**, *59*, 2544.
(3) Zalicki, P.; Zare, R. N. *J. Chem. Phys.* **1995**, *102*, 2708.
(4) Scherer, J. J.; Paul, J. B.; O'Keefe, A.; Saykally, R. J. *Chem. Rev.* **1997**, *97*, 25.
(5) Wheeler, M. D.; Newman, S. M.; Orr-Ewing, A. J.; Ashfold, M. N. R. *J. Chem. Soc., Faraday Trans.* **1998**, *94*, 337.
(6) Romanini, D.; Lehmann, K. K. *J. Chem. Phys.* **1993**, *99*, 6287.
(7) Yu, T.; Lin, M. C. *J. Am. Chem. Soc.* **1993**, *115*, 4371.
(8) Lin, M. C.; Yu, T. *Int. J. Chem. Kinet.* **1993**, *25*, 875.
(9) Yu, T.; Lin, M. C. *J. Am. Chem. Soc.* **1994**, *116*, 9571.
(10) Yu, T.; Lin, M. C. *J. Phys. Chem.* **1994**, *98*, 2105.
(11) Yu, T.; Lin, M. C. *J. Phys. Chem.* **1994**, *98*, 9697.
(12) Yu, T.; Lin, M. C. *J. Phys. Chem.* **1995**, *99*, 8599.
(13) Park, J.; Dyakov, I. V.; Mebel, A. M.; Lin, M. C. *J. Phys. Chem. A.* **1997**, *101*, 6043.
(14) Park, J.; Chakraborty, D.; Lin, M. C. *J. Phys. Chem.* **1999**, *103*, 4002.
(15) Park, J.; Burova, S.; Rodgers, A. S.; Lin, M. C. *J. Phys. Chem. A.* **1999**, *103*, 9036.
(16) Nam, G.-J.; Wensheng, X.; Park, J.; Lin, M. C. *J. Phys. Chem. A.* **2000**, *104*, 1233.
(17) Diau, E. W.; Yu, T.; Wagner, M. A. G.; Lin, M. C. *J. Phys. Chem.* **1994**, *98*, 4304.
(18) Atkinson, D. B.; Hudgens, J. W. *J. Phys. Chem. A.* **1997**, *101*, 3901.
(19) Atkinson, D. B.; Hudgens, J. W.; Orr-Ewing, A. J. *J. Phys. Chem. A.* **1999**, *103*, 6173.
(20) Atkinson, D. B.; Hudgens, J. W. *J. Phys. Chem. A.* **2000**, *104*, 811.
(21) Atkinson, D. B.; Hudgens, J. W. *J. Phys. Chem. A.* **1999**, *103*, 4242.
(22) Zhu, L.; Kellis, D.; Ding, C.-F. *Chem. Phys. Lett.* **1996**, *257*, 487.
(23) Cronin, T. J.; Zhu, L. *J. Phys. Chem.* **1998**, *102*, 10 274.
(24) Zhu, L.; Cronin, T.; Narang, A. *J. Phys. Chem. A.* **1999**, *103*, 7248.
(25) Zhu, L.; Cronin, T. J. *Chem. Phys. Lett.* **2000**, *317*, 227.
(26) Zhu, L.; Johnston, G. *J. Phys. Chem.* **1995**, *99*, 15 114.
(27) Tonokura, K.; Marui, S.; Koshi, M. *Chem. Phys. Lett.* **1999**, *313*, 771.
(28) Min, Z.; Wong, T.-H.; Quandt, R.; Bersohn, R. *J. Phys. Chem. A.* **1999**, *103*, 10 451.
(29) Ninomiya, Y.; Hashimoto, S.; Kawasaki, M.; Wallington, T. I. *Int. J. Chem. Kinet.* **2000**, *32*, 125.
(30) Yokelson, R. J.; Burkholder, J. B.; Fox, R. W.; Talukdar, R. K.; Ravishankara, A. R. *J. Phys. Chem.* **1994**, *98*, 13 144.
(31) In practice, it would be difficult to observe second-order kinetics using SKaR. Because the characteristic reaction time, $1/k[A]_0$, must be approximately the same as τ_0, the initial concentration, $[A]_0$, must be large. Furthermore, to ensure that the absorbance is not too large, the quantity $c\sigma[A]_0$ must be approximately equal to $1/\tau_0$, or σ must be small. We have not attempted to demonstrate second-order kinetics in this study of NO_3 radicals since the NO_3 self-reaction is slow, and the absorption cross section is large. In principle, however, one could do so in a more reactive system by generating a large radical concentration and using spectral features with small absorption cross sections.
(32) Brown, S. S.; Wilson, R. W.; Ravishankara, A. R. *J. Phys. Chem.* **2000**, *104*, 4976.
(33) Yao, F.; Wilson, I.; Johnston, H. *J. Phys. Chem.* **1982**, *86*, 3611.
(34) Swanson, D.; Kan, B.; Johnston, H. S. *J. Phys. Chem.* **1984**, *88*, 3115.
(35) Ravishankara, A. R.; Wine, P. H.; Smith, C. A.; Barbone, P. E.; Torabi, A. *J. Geophys. Res.* **1986**, *91*, 5355.
(36) Brown, S. S.; Talukdar, R. K.; Ravishankara, A. R. *J. Phys. Chem.* **1999**, *103*, 3031.
(37) Davidson, J. A.; Viggiano, A. A.; Howard, C. J.; Dotan, I.; Fehsenfeld, F. C.; Albritton, D. L.; Ferguson, E. E. *J. Chem. Phys.* **1978**, *68*, 2085.
(38) Burkholder, J. B.; Talukdar, R. K.; Ravishankara, A. R.; Soloman, S. *J. Geophys. Res.* **1993**, *98*, 22 937.
(39) There is some covariance between the two parameters k' and α_0; if α_0 was constrained to lie within +100/−70% of that in Figure 1b, it changed the best fit value for k' −50/+300% without visually degrading the fit. Nevertheless, for all traces at a given concentration of NO, the fit algorithm found the same value of k' and α_0 regardless of the initial guesses for these parameters. The fit procedure thus appears to be robust.
(40) Sander, S. P.; Friedl, R. R.; DeMore, W. B.; Golden, D. M.; Kurylo, M. J.; Hampson, R. F.; Huie, R. E.; Moortgat, G. K.; Ravishankara, A. R.; Kolb, C. E.; Molina, M. J. *Chemical Kinetics and Photochemical Data for Use in Stratospheric Modeling, JPL Publication 00-03*, Pasadena, CA, 2000.
(41) Torabi, A. *An Investigation of the Kinetics and Excited-State Dynamics of the Nitrate Free Radical*, Ph.D. Thesis, Georgia Institute of Technology, 1985.